REGULAR PAPER

Efficient Analysis of CFRP Cutting Force and Chip Formation Based on Cutting Force Models Under Various Cutting Conditions

Dong-Gyu Kim[1,2] · Seung-Han Yang[2]

Abstract

The cutting characteristics of unidirectional carbon fiber-reinforced plastic (CFRP) during zig-zag milling, which is the most used milling tool path in the industry, were analyzed. Cutting force and chip formation are the most useful indicators of cutting performance. Here, cutting force and chip formation were analyzed in up- and down-milling, then compared with those parameters in zig-zag milling. CFRP cutting force models for up- and down-milling were used for analysis of cutting force. Chip formations were predicted via simulations of fiber cutting angle. This simulation-based study overcame various experimental limitations regarding CFRP cutting force. The specific cutting forces of various fiber cutting angles were derived from cutting experiments involving unidirectional CFRP. The specific cutting forces decreased with increasing chip thickness. These results are similar to the size effect observed in metal machining. Cutting force analysis was performed with a focus on change in feed direction and rate of radial immersion. In zig-zag milling, the optimal feed direction rapidly changed at a radial immersion of 30%. At a radial immersion of 75%, the difference in cutting force related to the change in the feed direction was large. Type I (delamination-type) chip formation was dominant in the optimal feed direction because specific cutting force was lower in the Type I section than in regions of other chip formation types.

Keywords CFRP · Chip formation · Cutting force model · Down-milling · Tool path · Up-milling · Zig-zag milling

Abbreviations

h	Chip thickness [mm]
a_p	Axial depth of cut [mm]
f_z	Feed rate [mm/rev-tooth]
θ	Cutting tool rotation angle [°]
$\varnothing$	Fiber cutting angle [°]
φ	Fiber orientation angle [°]
φ_a	Absolute fiber orientation angle [°]
θ_s	Cutting tool entry angle [°]
θ_e	Cutting tool exit angle [°]
θ_c	Immersion angle range of cutting tool [°]
a_e	Radial depth of cut [mm]
D	Cutting tool diameter [mm]
f_d	Feed direction [°]
F_t, F_r	Tangential cutting force [N], radial cutting force [N]
F_x, F_y	Milling force in x-direction [N], milling force in y-direction [N]
K_t, K_r	Tangential specific cutting force [N/mm²], radial specific cutting force [N/mm²]
R	Cutting tool radius [mm]
N_t	Number of teeth on cutting tool
F_{up}, F_{down}	Up-milling resultant cutting force [N], down-milling resultant cutting force [N]
F_{sum}	Sum of resultant cutting forces [N

✉ Seung-Han Yang
  syang@knu.ac.kr

1 Advanced Cutting Tool Center, Daegu Mechatronics and Materials Institute, 3, Seongseogongdan-ro, Dalseo-gu, Daegu 42715, Republic of Korea

2 School of Mechanical Engineering, Kyungpook National University, 80, Daehak-ro, Buk-gu, Daegu 41566, Republic of Korea

1 Introduction

Carbon fiber-reinforced plastics (CFRPs) are increasingly used in high-value-added industries, such as aerospace, automotive, and renewable energy. The superior mechanical properties of CFRP are the driving force behind its increased use [1–3].

Generally, high precision and surface quality stabilization are essential when cutting CFRP parts. However, CFRP is a challenging material to cut because of characteristics such

as anisotropicity, inhomogeneity related to differences in the physical characteristics of fibers and polymers, and chip fragmentation [4]. These characteristics cause various cutting quality problems, including uncut fibers, fiber failures, fiber pull-out, delamination, and subsurface damage [5–7].

Extensive research has been conducted to solve these issues. First, attempts were made to analyze the cutting characteristics of CFRP via parametric studies [4, 5, 8–11]. Haddad et al. [4] evaluated the machined surface and chip according to cutting tool geometry and cutting conditions during CFRP trimming. They showed that the chip size was smaller than the theoretical size; the chip was fragmented and generated in the form of small particles. They also found that cutting tool geometry determined the chip shape. Hocheng et al. [5] investigated cutting force, quality, and cutting tool wear under various cutting conditions. They found that the cutting force increased at all fiber orientation angles when the feed rate was increased; cutting force in the direction parallel to the fiber was lower than cutting force in the orthogonal direction. Abrao et al. [8] examined how cutting tool geometry affected the delamination of glass fiber-reinforced plastic. They concluded that thrust force and delamination were not directly related; these parameters were affected by feed rate and cutting speed. Gaitonde et al. [9] experimentally analyzed drilling hole delamination. They found that delamination decreased with increasing cutting speed; the combination of feed rate and point angle significantly affected delamination. Gaugel et al. [10] analyzed tendencies of cutting tool wear and delamination through experiments involving uncoated carbide drills and coated drills, respectively. They found that diamond coating could significantly increase cutting tool performance; one- and two-dimensional delamination factors differed because of the anisotropic nature of CFRP. Geier [11] analyzed cutting force according to cutting condition (e.g., up- and down-milling of unidirectional CFRP). In that study, multiple-order polynomial models were developed to identify the fiber orientation that corresponded to the minimum cutting force. However, the study was experiment-based, and it provided few insights regarding CFRP cutting mechanisms in different experimental paradigms.

Methods to predict the cutting force of CFRP have also been explored [5, 12–15]. Sheikh-Ahmad et al. [12] predicted the cutting force based on specific cutting energy functions. They found that, compared with regression techniques, the neural network was a better simulation method. Mullin et al. [13] predicted the cutting forces of unidirectional and multidirectional CFRP by deriving cutting force coefficients from the mean cutting force. Ning et al. [14] determined the specific cutting force by simplifying chip thickness to a uniform value; the mean cutting force was predicted during milling. Wang et al. [15] attempted to predict the periodic fluctuations of the CFRP milling cutting force,

then compensated the cutting force through a frequency response function test. Kim et al. [16] used a CFRP cutting force model to optimize the cutting force and demonstrated that the model could be used to optimize feed direction. Existing literature indicates that the derivation of a specific cutting force within a CFRP cutting force model is complex; thus, further research is needed to improve its accuracy and efficiency. However, there is limited research focused on cutting force optimization using a model that includes the influence of tool path.

Additionally, efforts are underway to improve machining efficiency through the addition of advanced technologies such as ultrasonic [17, 18], cryogenic [19–21], and preheating [22] machining. However, commercial adoption of these advanced technologies has not been achieved.

Critical indicators of machinability in the above studies were cutting force and chip formation [4, 5, 8, 11–16]. Therefore, many studies have attempted to improve CFRP machinability through the development of a cutting force model [17–23]. However, among the studies related to CFRP cutting force and chip formation, there has been limited emphasis on the tool path. With respect to metals, extensive research has been carried out regarding the effect of tool path on cutting characteristics; difficult-to-cut materials, new materials, new tool development, and multi-axis machining remain active research topics [23–30]. With respect to CFRP, some studies have examined the effect of tool path on cutting force and delamination [11, 31] and on hole machining using a helical tool path [32]. However, there is minimal literature regarding the cutting characteristics of a typical tool path, such as zig-zag milling. Because cutting characteristics substantially vary depending on cutting conditions in CFRP machining, there is a need to analyze the behavior of cutting characteristics according to various zig-zag milling conditions.

With respect to CFRP, the fiber cutting angle—influenced by cutting tool diameter, fiber orientation angle, radial depth of cut, and feed direction—affects cutting force and chip formation. Additionally, because repetitive up- and down-milling occurs during zig-zag milling of CFRP, the cutting force and chip formation during up- and down-milling must also be considered. Numerous variables must be considered for cutting force analysis of CFRP zig-zag milling; the number of experiments required is infeasible.

This study analyzed cutting force and chip formation in zig-zag milling using the CFRP cutting force model. First, we derived the CFRP zig-zag milling cutting force model for cutting force analysis via simulation, rather than experimentation. Second, we investigated zig-zag milling cutting force trends by analysis of up- and down-milling, followed by comparison of those results with the results of zig-zag milling. Third, we categorized the chip formation type through analyses of fiber cutting angles. Zig-zag milling is the most representative tool

path in rough milling; however, CFRP cutting force analysis was not performed because of the excessive number of variables. This study explored cutting force trends during CFRP zig-zag milling under various conditions. Our findings suggest that the field of CFRP machining could achieve productivity improvement and cutting force stabilization by determining the optimal feed direction during zig-zag milling.

2 CFRP Milling Cutting Mechanism

2.1 CFRP Zig-Zag Milling

In general, zig-zag milling involves repeated up- and down-milling. The chip thickness h is a function of the feed rate f_z [mm/rev-tooth] and cutting tool rotation angle θ (Eq. (1)). Here hda_p is the chip area [mm²] of one disk when the axial depth of cut is divided into infinitesimal depths.

$$h = f_z sin\theta$$
$$hda_p = da_p \cdot f_z sin\theta \tag{1}$$

Figure 1 presents the results of chip area calculations for up- and down-milling using Eq. (1). During up-milling, the chip area is 0 at the cutting start point and maximum at the endpoint (Fig. 1a). The results for down-milling are opposite to the results of up-milling (Fig. 1b). As the cutting force for isotropic materials, such as metals, is proportional to both the chip area and specific cutting force, the cutting force behavior is generally similar to that of the chip area.

The fiber cutting angle $\varnothing$, which is the angle between the cutting tool tooth and the fiber, continues to change during cutting tool rotation. The absolute fiber orientation angle φ_a is the angle between the fiber and the x-direction; it is determined by the direction in which the CFRP is fixed to the machine tool table. The fiber cutting angle and chip thickness differ during up- and down-milling. For example, consider an absolute fiber orientation angle of 30°, and a radial depth of cut a_e that is 50% of the cutting tool diameter (i.e., 50% radial immersion). During up-milling, the fiber cutting angle begins at 150° and

ends at 60°; during down-milling, the fiber cutting angle begins at 60° and ends at 150° (Fig. 2). These findings indicate that CFRP milling is considerably more complex than metal machining.

Equation (2) describes the fiber cutting angle as a function of cutting tool rotation angle and fiber orientation angle φ. Here, the fiber orientation angle lies between the feed direction f_d and the fiber. The fiber orientation angle is influenced by feed direction.

$$
\begin{aligned}
\varnothing &= (\theta - \varphi)° + 180° \quad for \quad -180° < \theta - \varphi \leq 0° \\
\varnothing &= (\theta - \varphi)° \qquad\qquad for \qquad 0° < \theta - \varphi < 180° \\
\varnothing &= (\theta - \varphi)° - 180° \quad for \qquad 180° < \theta - \varphi
\end{aligned} \tag{2}
$$

The angle at which the cutting tool tooth begins cutting is θ_s; the angle at which the cutting ends is θ_e, which can be determined using Eq. (3). a_e is the radial depth of cut, and D is the cutting tool diameter.

$$
\begin{aligned}
\theta_e &= 180° \\
\theta_s &= 180° - \left\{ \left(arc\cos\left(1 - \frac{a_e}{D}\right)\right) \times \frac{180}{\pi} \right\} \\
\theta_c &= \theta_e - \theta_s
\end{aligned} \tag{3}
$$

2.2 CFRP Cutting Force Model

The prediction of cutting force during milling requires knowledge of the specific cutting force and prediction of the chip removal area over an infinitesimal interval of time. The chip removal area can be calculated based on cutting tool rotation angle and feed rate. The chip removal area per infinitesimal section of cutting tool tooth can be calculated according to the cutting conditions [33]. This chip removal area can be used to predict tangential, radial, and axial cutting forces (Eq. (4)). Here, dF_t, dF_r, and dF_a are the tangential, radial, and axial cutting forces of the infinitesimal disk of the cutting tool tooth, respectively; K_t, K_r, and K_a are the specific cutting forces in each direction. The chip area hda_p can be calculated using Eq. (1).

Fig. 1 Chip area during up- and down-milling (cutting tool diameter: 20 mm; radial depth of cut: 10 mm). **a** Up-milling and **b** down-milling
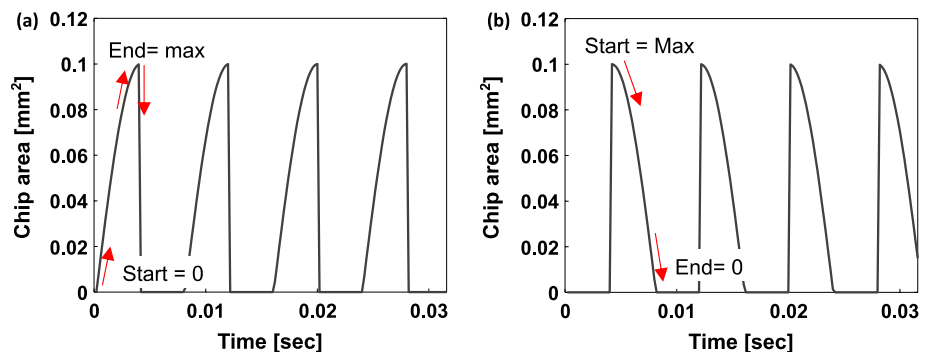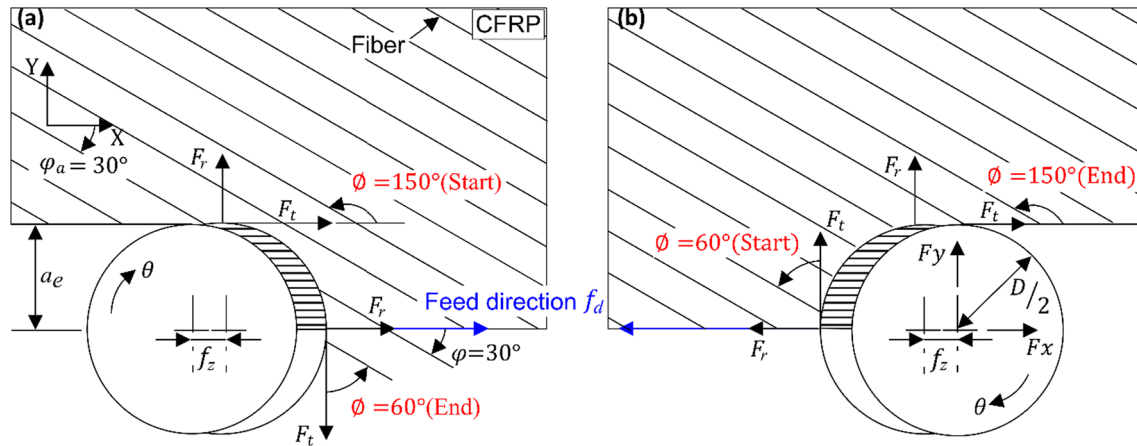
Fig. 2 Schematic illustration of geometrical relationship between CFRP and cutting tool during up- and down-milling. **a** Up-milling and **b** down-milling

$$dF_t = K_t h da_p$$
$$dF_r = K_r h da_p \tag{4}$$
$$dF_a = K_a h da_p$$

The cutting force in cylindrical coordinates can be expressed as the cutting force in Cartesian coordinates via coordinate transformation (Eq. 5), as follows:

$$\begin{bmatrix} dF_x \\ dF_y \\ dF_z \end{bmatrix} = \begin{bmatrix} \cos\theta & \sin\theta & 0 \\ -\sin\theta & \cos\theta & 0 \\ 0 & 0 & 1 \end{bmatrix} \begin{bmatrix} dF_t \\ dF_r \\ dF_a \end{bmatrix} \tag{5}$$

Continuous cutting force can be predicted by dividing the cutting tool rotation angle into infinitesimal angles, calculating the corresponding cutting force using Eq. (4), and then summing the results. Continuous cutting force can be derived from the amount repeated in units of the sampling rate (Eq. 6). The resultant cutting force in the x-, y-, and z-directions is F. Here, k is the index number indicating the number of cutting edges, N_t is the number of teeth of the cutting tool, l is the total number of disks in the axial depth of cut, and j is the index number.

$$F_x = \sum_{k=1}^{N_t} \sum_{j=1}^{l} dF_{x_{kj}}$$

$$F_y = \sum_{k=1}^{N_t} \sum_{j=1}^{l} dF_{y_{kj}}$$

$$F_z = \sum_{k=1}^{N_t} \sum_{j=1}^{l} dF_{z_{kj}} \tag{6}$$

$$F = \sum_{k=1}^{N_t} \sum_{j=1}^{l} \sqrt{dF_{x_{kj}}^2 + dF_{y_{kj}}^2 + dF_{z_{kj}}^2}$$

According to Eq. (2), the fiber cutting angle is affected by the immersion angle ($\theta_s \sim \theta_e$) and the fiber orientation angle. Therefore, changes in these two values can also influence the fiber cutting angle. The immersion angle during cutting can be expressed as a function of cutting tool diameter and radial depth of cut (Eq. (3)). Additionally, the fiber orientation angle can be defined as a function of the absolute fiber orientation angle and the feed direction. Therefore, during CFRP cutting, the fiber cutting angle—which significantly affects cutting force and chip formation—varies according to cutting tool diameter, radial immersion, absolute fiber orientation angle, and feed direction in milling. Although the fiber cutting angle is difficult to control, the fiber orientation angle can be easily adjusted by modifying the feed direction. Although the machining area and fixture orientation determine the absolute fiber orientation angle, the fiber orientation angle can be changed via modification of the feed direction when designing the CNC code. It is generally easy to modify the feed direction in a process focused on removal of workpiece volume, such as face milling [16].

Zig-zag milling is mainly used in the face-milling process; it comprises repeating cuts during up- and down-milling. Up- and down-milling feed directions are always opposite to each other. The fiber cutting angle determined by changing the feed direction (clockwise) (expressed by the term ($\theta - \varphi$) in Eq. (2)) is modified to $(\theta - (\varphi_a - f_d))$. Moreover, the cutting characteristics of both up- and down-milling, as determined by changing the feed direction, should be considered simultaneously.

When analyzing changes in cutting force according to feed direction, the range of fiber cutting angle depends on radial immersion; thus, radial immersion should also be considered. Cutting force must be analyzed through the division of radial immersion and feed direction in various conditions. The cutting force in each feed direction is derived

at each radial immersion. Comparison of cutting force in each feed direction at one radial immersion can be used to determine minimum cutting force. The cutting force can be analyzed by repeating this process for all radial immersions ranging from 0 to 100%. This analysis is conducted by assigning an index number to each radial immersion and feed direction (Fig. 3a), and the cutting forces during up- and down-milling are predicted (Fig. 3b); the immersion angle varies between up- and down-milling. Determination of the optimal feed direction index m that corresponds to the index q of each radial immersion allows identification of the feed direction in which the cutting force is minimized.

(a) Flow chart to identify optimal feed direction

(b) Flow chart to predict CFRP cutting force
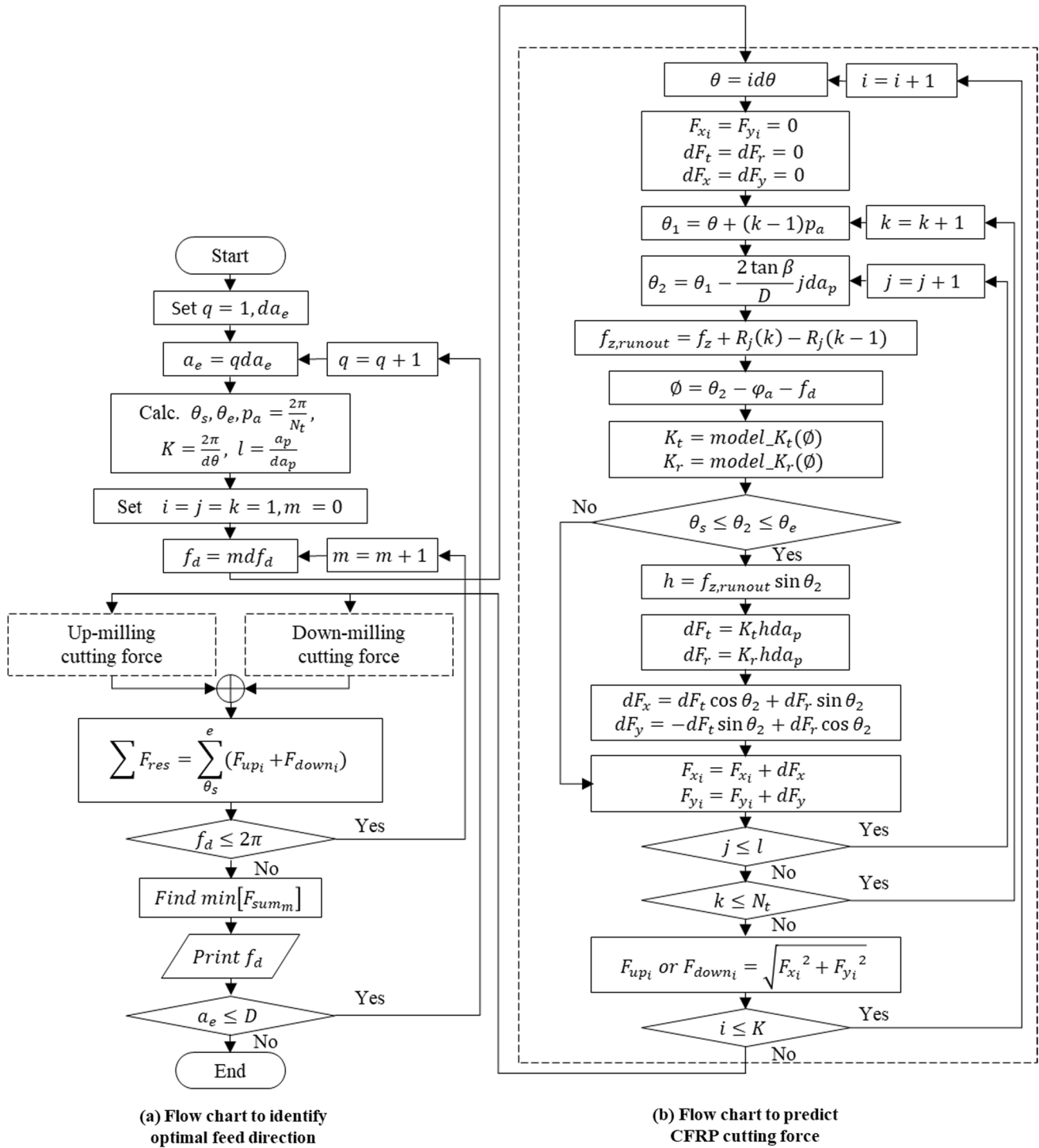
Fig. 3 Flow charts for analysis of cutting force according to feed direction and radial immersion

2.3 Prediction of Chip Formation Type

The five types of chip formation in unidirectional CFRP machining are determined by the fiber cutting angle and the rake angle of the cutting tool tooth. Figure 4 shows chip formation under the cutting tool conditions used in this study. Type I is a delamination-type chip; Type II is a fiber-buckling chip, which occurs when the rake angle is negative. The polycrystalline diamond (PCD) milling tool used in this study has a positive rake angle; thus, Type II chip formation does not occur. In Type III, continuous chips are formed by shearing, similar to chip formation that occurs during metal machining. Type IV is similar to Type III, but discontinuous chips are formed. In Type V, macro fractures of the fiber are dominant because of extensive elastic bending [34].

Figure 4 shows the classification of chip formation type in our experimental conditions. Figure 4a illustrates the classification according to fiber cutting angle: 0°–45° corresponds to a Type I delamination-type chip, 45°–90° corresponds to a Type V macro fracture chip, 90°–120° corresponds to a Type IV discontinuous chip, and 120°–180° corresponds to a Type III continuous chip. This chip formation classification scheme applies when the cutting tool rake angle is 10°; however, the chip formation type is varied by alteration of the rake angle. Figure 4b illustrates the up- and down-milling chip formation types, along with chip area, when the fiber orientation angle is approximately 120° and radial immersion is 50%. Using Eqs. (1) and (2), the chip area for each chip formation type can be determined according to cutting tool rotation angle. During up-milling, Type I chip formation is initially observed; Type V formation is observed as the cutting tool rotates, and Type IV formation is observed when the cutting tool exits the workpiece. At this time, the Type I chip area is smallest, whereas the Type IV chip area is largest. During down-milling, chip formation begins with Type IV, progresses to Type III, and finishes with Type I.

The Type IV chip area is smallest, whereas the Type III chip area is largest. Because this model can predict the fiber fracture mode during cutting, engineers can estimate cutting characteristics that are difficult to confirm prior to cutting.
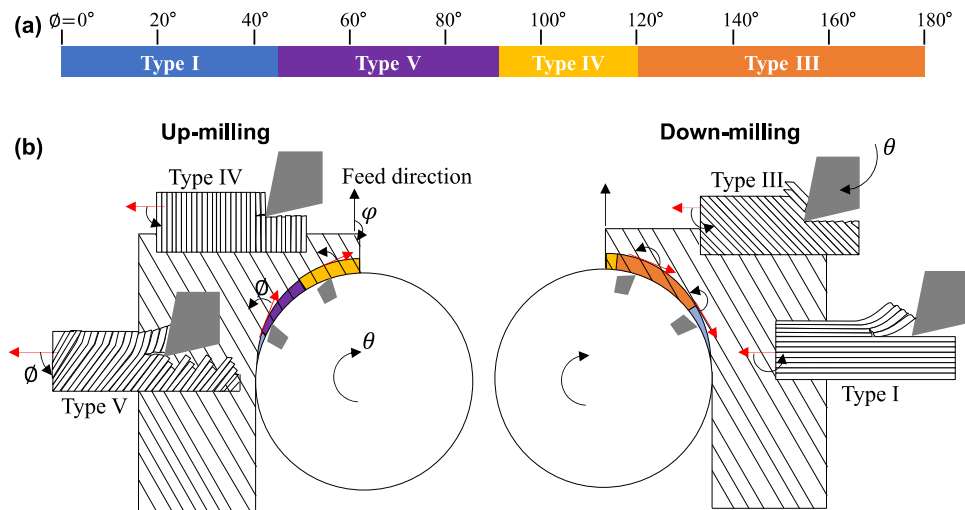
2.4 Experiments

The specific cutting force is usually a scalar value for metals, whereas it is a function of the fiber cutting angle for CFRP. The chip generation mechanism and fracture mode vary according to the fiber cutting angle, as discussed above. The chip area and specific cutting force are required to predict the cutting force using Eq. (4), and the chip area can be calculated according to Eq. (1). However, the specific cutting force differs according to the specifications of the CFRP; thus, it was derived by experimentation.

To derive the specific cutting force, machining tests were conducted on unidirectional CFRP with fiber orientation angles of 0°, 30°, 60°, 90°, 120°, and 150° using a PCD milling tool. The cutting force was measured using a tool dynamometer (model 9257B; kistler.com, Switzerland) at a sampling rate of 5000 Hz (Fig. 5a). Toray yarn T700 12 k prepreg (thickness, 0.137 mm) was used as the CFRP. The cutting tool was a two-tooth PCD milling tool with rake angle of approximately 9°, relief angle (clearance angle) of 20°, and helix angle of 0°. The corner radius of the cutting tool tooth edge, which affects CFRP cutting characteristics, was maintained using a Lasertec 20 machine (dmgmori.com, Germany). The PCD (CFW grade; iljindiamond.co.kr, South Korea) was brazed to a carbide body (Fig. 5b).

The derivation of a specific cutting force requires measurements of cutting force in the tangential, radial, and axial directions. However, the fixed tool dynamometer can generally measure cutting force in the x-, y-, and z-directions (Fig. 5c). These values must be converted into the cutting force in a cylindrical coordinate system

Fig. 4 CFRP chip formation. **a** Classification of chip formation type according to fiber cutting angle and **b** chip formation type during up- and down-milling
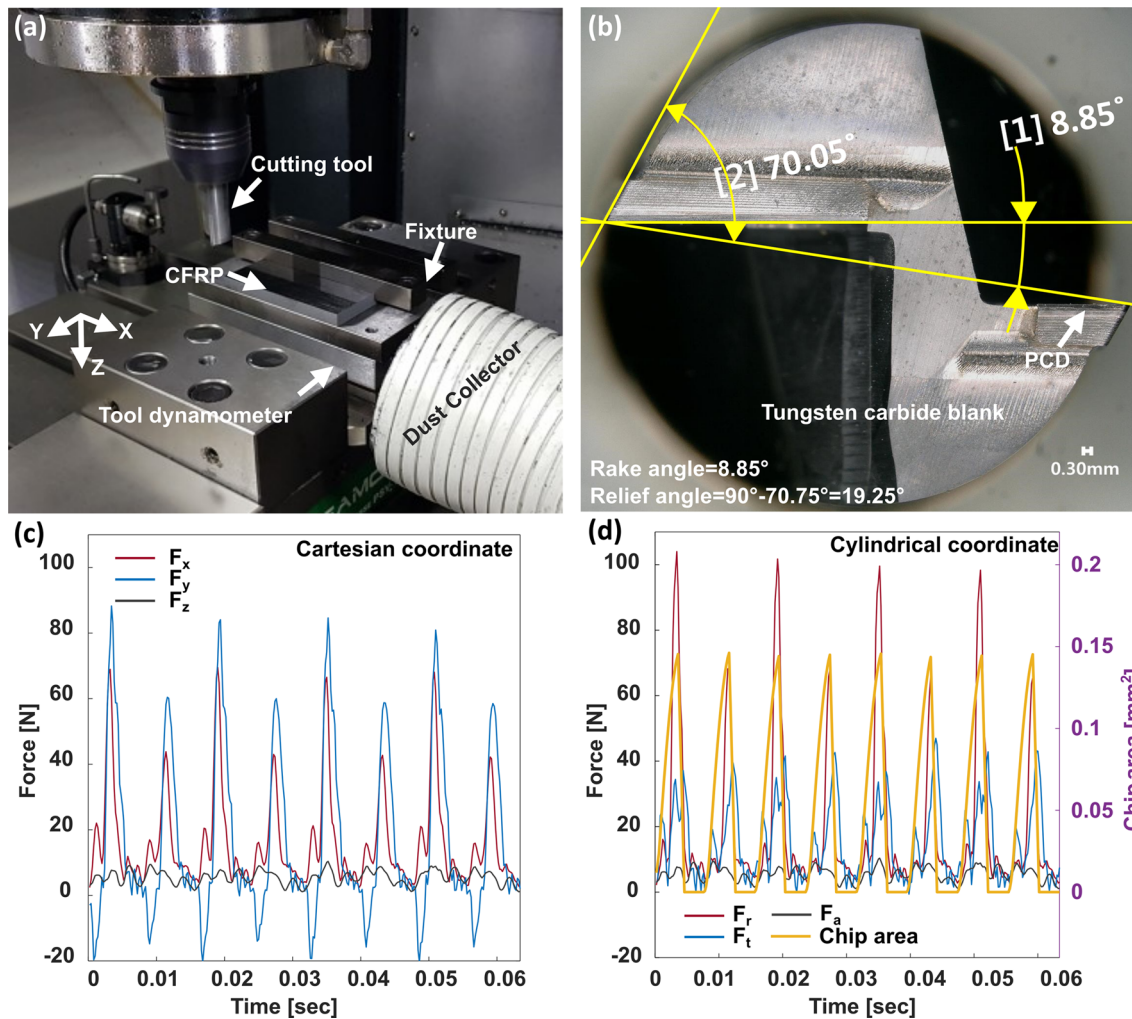
Fig. 5 Experimental setup and analysis for determination of specific cutting force

by using the inverse matrix of Eq. (5). Subsequently, the specific cutting force can be derived by matching the phase of the cutting force with the chip area, based on the cutting tool rotation angle (Fig. 5d). Finally, the cutting force can be converted into a specific cutting force according to the fiber cutting angle using Eqs. (2) and (3).

Table 1 shows the milling test cutting conditions used in this study. First, to derive a specific cutting force, 10 mm was set as the radial depth of cut (50% radial immersion); cutting experiments were performed at six fiber orientation angles. The axial depth of cut was 2 mm, and the cutting speed was 250 m/min. The cutting force model shown in Fig. 3b was

Table 1 Cutting conditions for the milling test

Parameter	Specific cutting-force derivation	Cutting force model validation
Rotational speed [rpm]	3776	2547, 3776
Cutting speed [m/min]	250	160, 250
Feed rate [mm/min]	189, 378, 567	127.3, 189, 378, 567
Up-/down-milling	Up	Up, down
Radial/axial depth of cut [mm]	10/2	2–10/1, 2
Cutting tool	20 mm diameter, two-tooth PCD milling tool	20 mm diameter, two-tooth PCD milling tool
Material and fiber orientation angle [°]	UD CFRP 0, 30, 60, 90, 120, 150	UD CFRP 0, 30, 60, 90, 120, 150

created using the derived specific cutting force. The cutting force model was validated by up- and down-milling, and the predicted and experimental values were compared. After the cutting force model had been constructed and its reliability had been confirmed, the changes in cutting force according to feed direction and radial immersion were determined; conditions with minimal cutting force were established as shown in Fig. 3a. The optimal feed directions were derived for up- and down-milling, as well as zig-zag milling.

3 Results and Discussion

3.1 Cutting Force Model

Figure 6 presents the specific cutting force derived after the cutting experiment under the conditions listed in Table 1. Figure 6a shows the specific cutting force in the radial direction, whereas Fig. 6b shows the specific cutting force in the tangential direction. The results for each feed rate are shown. The specific cutting force in the radial direction is reduced at a fiber cutting angle of 0°–40°, increases from 40° to 120°, and then decreases to 180°. The specific cutting force in the tangential direction is reduced at a fiber cutting angle of 0°–40°; it rapidly increases from 40° to 60°, along with an increase in variance. Then, the force plateaus from 60° to 120°, and finally decreases to 180°. Variance is larger in the tangential direction than in the radial direction; the difference rapidly increases around the fiber cutting angle range of 40°–90°. This difference arises because the fiber cutting angle considerably influences CFRP cutting characteristics. Because this influence has strong effects on chip formation type, cutting force magnitude, and fluctuation, the specific cutting force is also affected [34].

The specific cutting force varies according to feed rate. As the feed rate increases, the overall specific cutting force decreases for both radial and tangential directions. This result is similar to the size effect phenomenon observed in metal machining: the specific cutting force increases as the chip thickness decreases, whereas the specific cutting force decreases as the chip thickness increases. As the feed rate increases, the specific cutting force is reduced because a thick chip is used to derive the specific cutting force for the same fiber cutting angle. The size effect is not apparent at the fiber cutting angle of 0°–40°, but it is evident after 40°. From 0° to 40°, chip formation by delamination (rather than machining) is dominant. Therefore, no size effect is expected during machining.

To predict CFRP cutting force, the specific cutting force should be expressed as a function of the fiber cutting angle. Generally, methods such as a simple sine function or polynomial regression are used because the specific cutting force of CFRP can be approximated by the sine function of the fiber cutting angle. In this study, a specific cutting force model was derived using a simple sine function (Eq. (7)), and a size effect term was generated according to the chip thickness. Here, a, b, and c are coefficients that represent the change in specific cutting force according to fiber cutting angle; d is the coefficient that expresses the exponential function related to the size effect.

$$K = (a + b \cdot \sin(2\varnothing + c))h^d \tag{7}$$

The specific cutting force varies periodically with the fiber cutting angle, and is the same at 0° and 180°. To deal with differences in specific cutting force between these angles, the sine function is utilized. Differences can occur if the fiber cutting angle is directly included in the
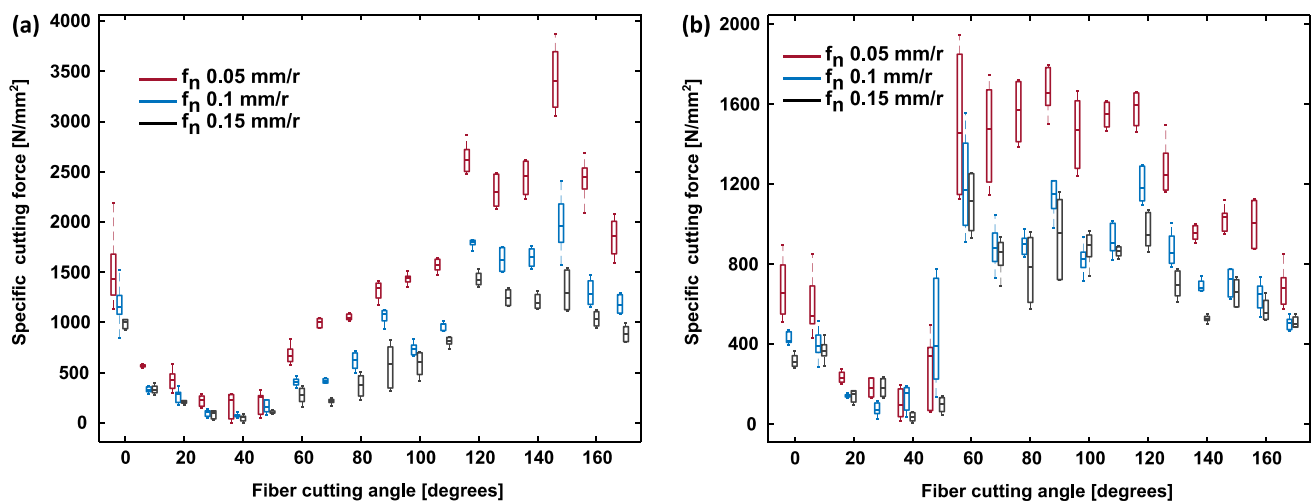

Fig. 6 Specific cutting forces. **a** Radial and **b** tangential

regression model. The coefficient d is negative because of the size effect, and the specific cutting force decreases as the chip becomes thicker but increases as the chip becomes thinner. Higher absolute values of coefficient d indicate greater sensitivity of the specific cutting force to changes in chip thickness. Table 2 shows the coefficients for specific cutting forces.

Figure 7 shows the results of fitting the specific cutting force using Eq. (7). The R-squared value (R^2) was 0.90 for the radial direction, whereas it was 0.77 for the tangential direction. Figure 5 shows that in the tangential direction, when the feed rate is slowed, the variance and specific cutting force rapidly increase at the fiber cutting angle of 40°–90°. Moreover, there is a substantial difference in variance according to the feed rate. These variance and size effects resulted in large errors in fitting results in the tangential direction.

Figures 8 and 9 present the cutting force prediction results for up- and down-milling using the specific cutting force model with the cutting conditions listed in Table 1, validated for each feed rate. The shape of the cutting force waveform and the maximum and minimum values can be adequately predicted at all fiber orientation angles.

3.2 Cutting Force Variation According to Feed Direction and Radial Immersion

Figure 10 shows the cutting force behavior according to the change in the feed direction and radial immersion at the

Table 2 Coefficients of the specific cutting force

Specific cutting force [N/mm²]	Coefficients			
	a	b	c	d
K_r	116.4	100.6	3.084	−0.6056
K_t	115.2	71.52	−2.188	−0.5322

absolute fiber orientation angle of 0°, as determined using the cutting force model. This figure considers up- and down-milling separately. Red dots indicate the feed direction where the cutting force is lowest at a particular radial immersion. During both up- and down-milling, as the radial immersion increases in each feed direction, the chip removal volume increases; this leads to an increase in cutting force. Because the cutting tool immersion angle and chip thickness differ between up- and down-milling, the resultant cutting force is generally different. Although the chip removal volumes are identical for a particular radial immersion, there is a substantial difference in cutting force according to the feed direction. This difference is caused by changes in the range of the fiber cutting angle according to feed direction. During up-milling, the resultant cutting force is high in the feed direction, at approximately 50°–100°; during down-milling, the force is low.

Figure 11 presents the optimal feed direction corresponding to the lowest cutting force for each condition (red dots in Fig. 10). This was derived using the flow charts shown in Fig. 3; it is the feed direction in which cutting force is minimized when cutting at the absolute fiber orientation angle of 0°. The slope of the optimal feed direction according to radial immersion is steeper than the slope of the optimal feed direction according to feed rate. These values can be used in various radial immersions and feed rates when selecting the feed direction and generating G codes. Variations in cutting force related to radial immersion are more sensitive than changes in feed rate, and the gradient according to change in the optimal feed direction is generally constant.

Table 3 shows the optimal feed directions for radial immersions of 5% and 100%, as well as feed rates of 0.02 and 0.2 mm/r. At 0.02 mm/r, the changes in optimal feed direction according to radial immersion are 70° (−37° to 33°) for up-milling and 76° (33° to 109°) for down-milling. At 0.2 mm/r, these changes are 50° (− 19° to 49°) for up-milling and 78° (49°–127°) for down-milling. The gradient
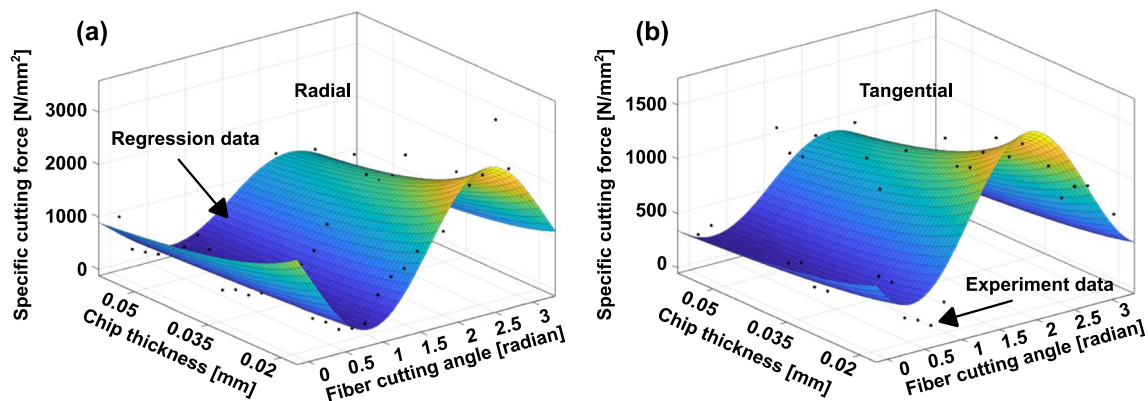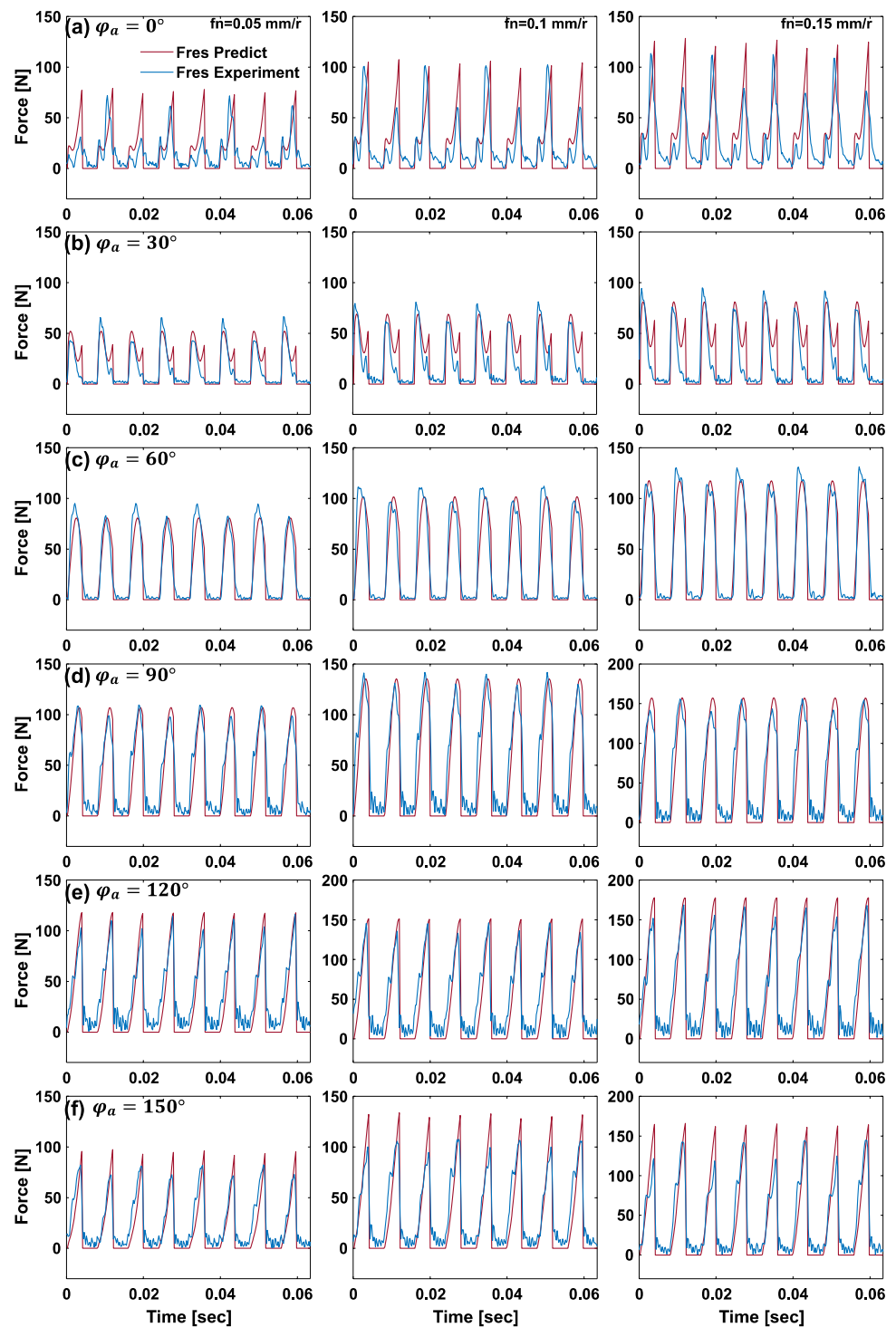

Fig. 7 Fitting of specific cutting force. **a** Radial direction and **b** tangential direction

**Fig. 8** Comparison of real (experimental) and predicted up-milling cutting forces

of change in optimal feed direction according to radial immersion is larger for down-milling than for up-milling. Therefore, a change in radial immersion during down-milling has considerably greater effect on the optimal feed direction, compared with a change during up-milling. However, according to the feed rate, the optimal change in feed direction is identical (18°) for both up- and down-milling at 5%

radial immersion. Even when the radial immersion is 100%, the change is 16° for both up- and down-milling conditions.

The optimal feed direction according to radial immersion and feed rate was fitted via polynomial regression. A reliable, optimal feed direction model with $R^2 > 0.99$ was identified for both up- and down-milling. Therefore, optimal feed direction models could be established using this regression

Fig. 9 Comparison of real (experimental) and predicted down-milling cutting forces
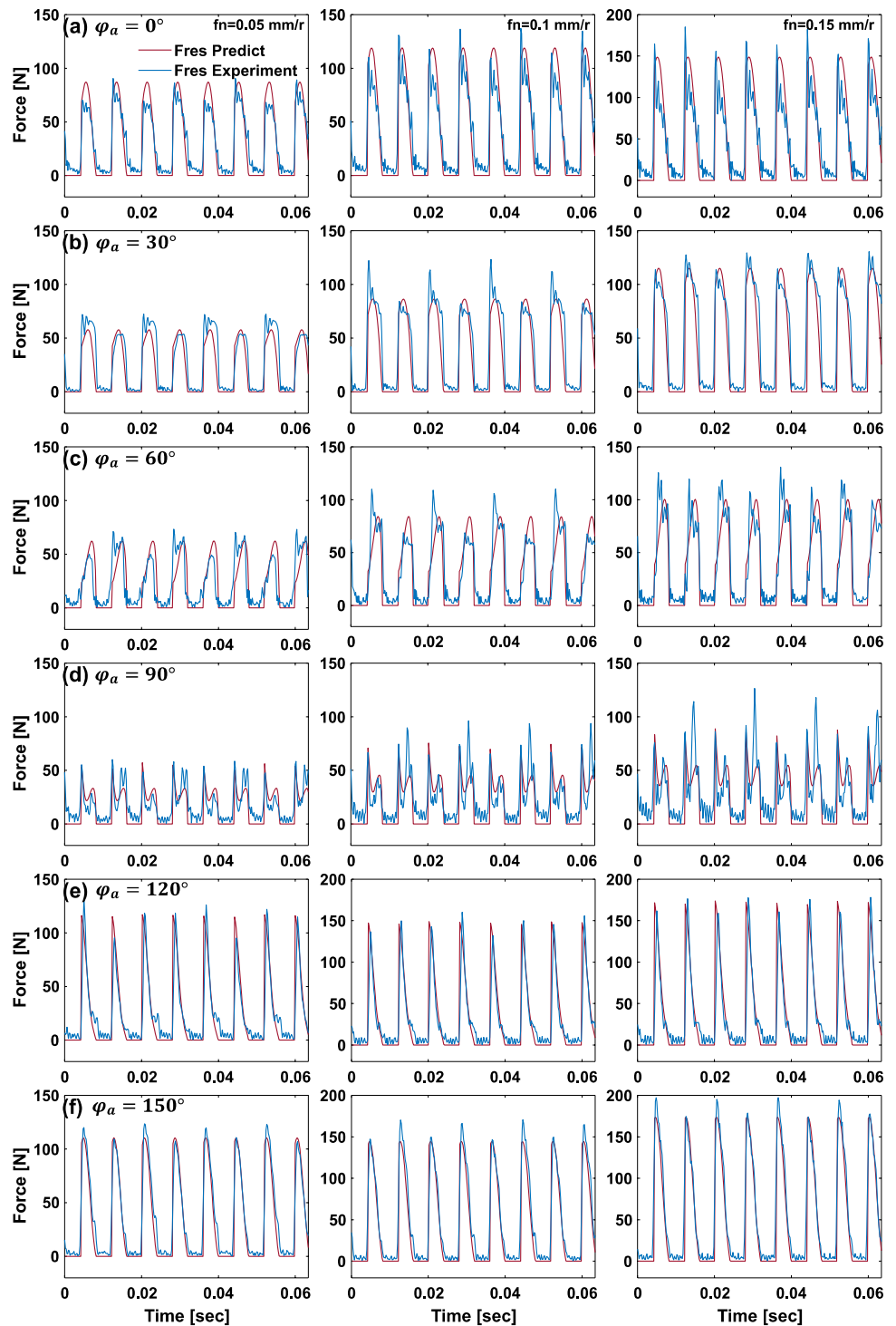
approach for different types of CFRPs, which would be useful when designing G code.

Figure 12 presents the difference, expressed as a percentage (reduction ratio)), between the maximum and minimum cutting forces occurring in the feed direction for both up- and down-milling. This value represents the extent to which cutting force can be reduced in each condition. For both up- and down-milling, lower radial immersion and lower feed rate result in greater reductions in cutting force. The rate of cutting force reduction is important for finishing. However, these results are calculated as a cutting force percentage. The values are larger in the roughing condition (i.e., high radial immersion, high feed rate) when calculated as an absolute value of the cutting force.
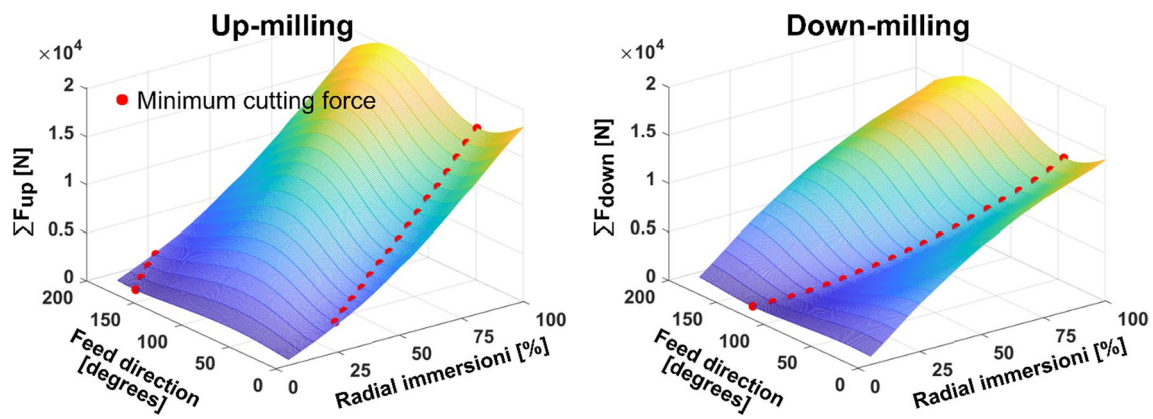
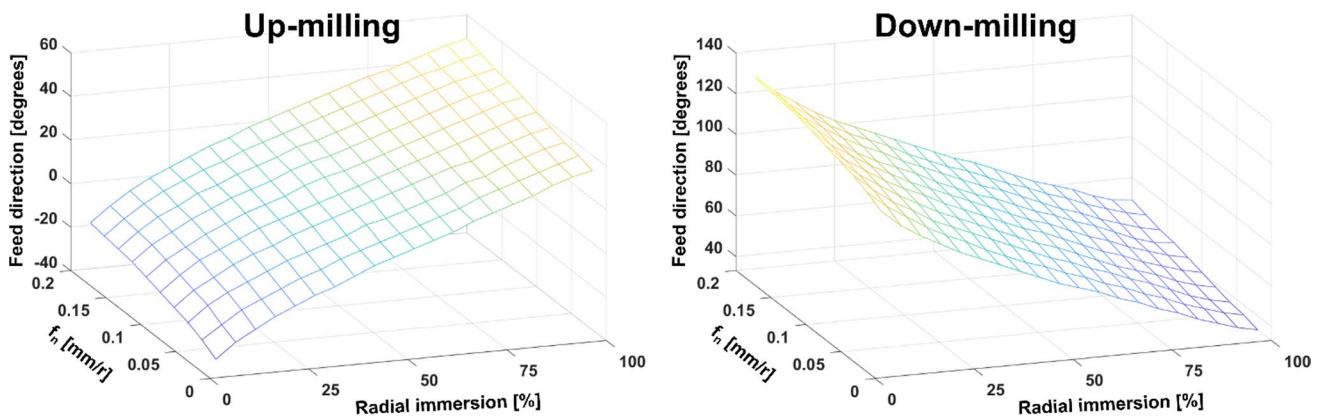**Fig. 10** Resultant cutting force as a function of feed direction and radial immersion

Fig. 11 Optimal feed direction as a function of radial immersion and feed rate

Table 3 Optimal feed directions under various cutting conditions

Radial immersion (%)/f_n [mm/r]	Optimal feed direction [°]	
	Up milling	Down milling
5/0.02	− 37 (143)	109
100/0.02	33	33
5/0.2	− 19 (161)	127
100/0.2	49	49

Figure 13 presents the cutting force as a function of feed direction and radial immersion for zig-zag milling. The total cutting force is the sum of the cutting forces of up- and down-milling during zig-zag milling. The optimal feed direction (red dots) rapidly changes from 111° to 27° after 30% radial immersion. For 0–30% radial immersion, the change in cutting force according to feed direction is unclear, although the change is evident after 30%. This finding contrasts with the results shown in Fig. 10, where the

optimal feed direction follows a continuous curve. Figure 14 shows the optimal feed direction for each condition depicted in Fig. 13. For all feed rates, a sharp change in the optimal feed direction occurs at 30% radial immersion, as discussed above.

Figure 15 shows the reduction ratio results for zig-zag milling. The reduction ratio decreases up to 30% radial immersion; after 30%, it exhibits a parabolic form. The reduction ratio is largest at 75% radial immersion: 47.5% at the feed rate of 0.02 mm/r and 30.8% at 0.2 mm/r. For up- or down-milling, lower radial immersion results in a higher reduction ratio. In zig-zag milling, the reduction ratio increases from 30% radial immersion and reaches a maximum at 75%, which is a roughing condition. Cutting force optimization is more frequently required in roughing than in finishing, where quality is important. These findings indicate that the use of tool path optimization in zig-zag milling is more appropriate than the use of up- or down-milling alone.
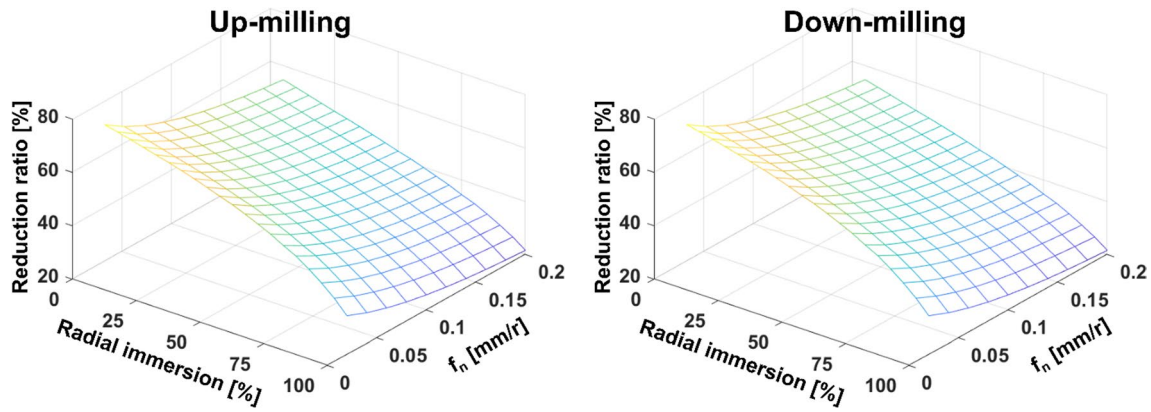
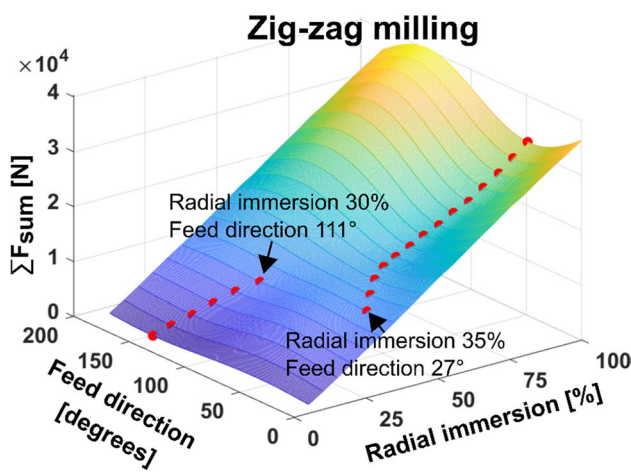**Fig. 12** Reduction ratio of cutting force as a function of radial immersion and feed rate

Fig. 13 Resultant cutting force as a function of feed direction and radial immersion during zig-zag milling
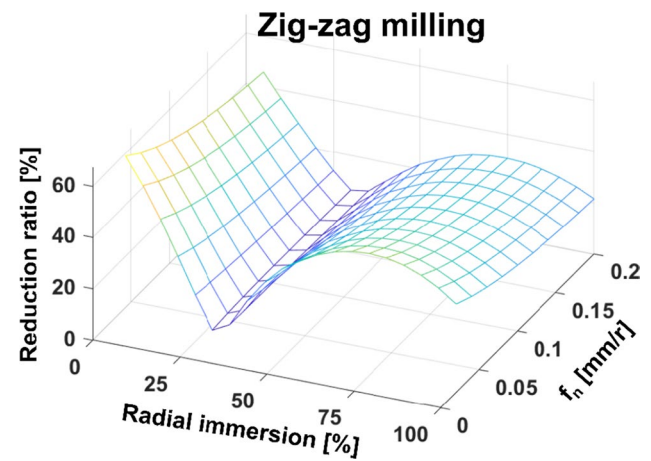

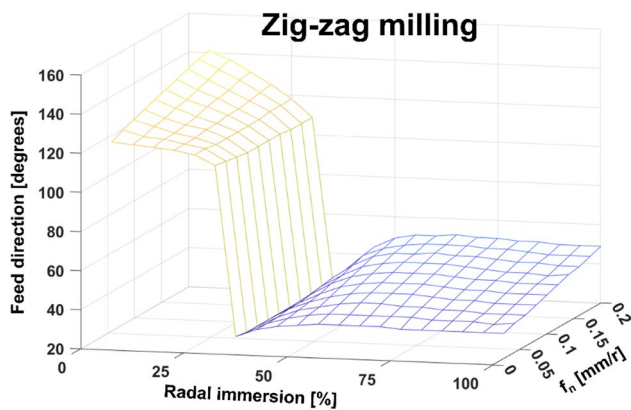**Fig. 15** Reduction ratio of cutting force as a function of radial immersion and feed rate in zig-zag milling

Fig. 14 Optimal feed direction as a function of radial immersion and feed rate for zig-zag milling

3.3 Chip Formation Type According to Tool Path

Figure 16 shows the chip areas removed in the optimal feed direction. First, we present the results of up- and down-milling alone [Fig. 16a] followed by the results of zigzag milling [Fig. 16b]. Zig-zag milling involves sequential up- and down-milling; we define up-and down-milling during zigzag milling as "zig-zag up-milling" and "zig-zag down-milling", respectively. Figure 16a presents the results of classifying the chip area according to the type of chip when machining with the optimal feed direction in up- and down-milling. The type is determined by the fiber cutting angle during chip removal, according to the cutting tool immersion angle. Type I chip formation is dominant in both up- and down-milling, whereas Type V formation has the smallest proportion. Figure 6 shows that the specific cutting force
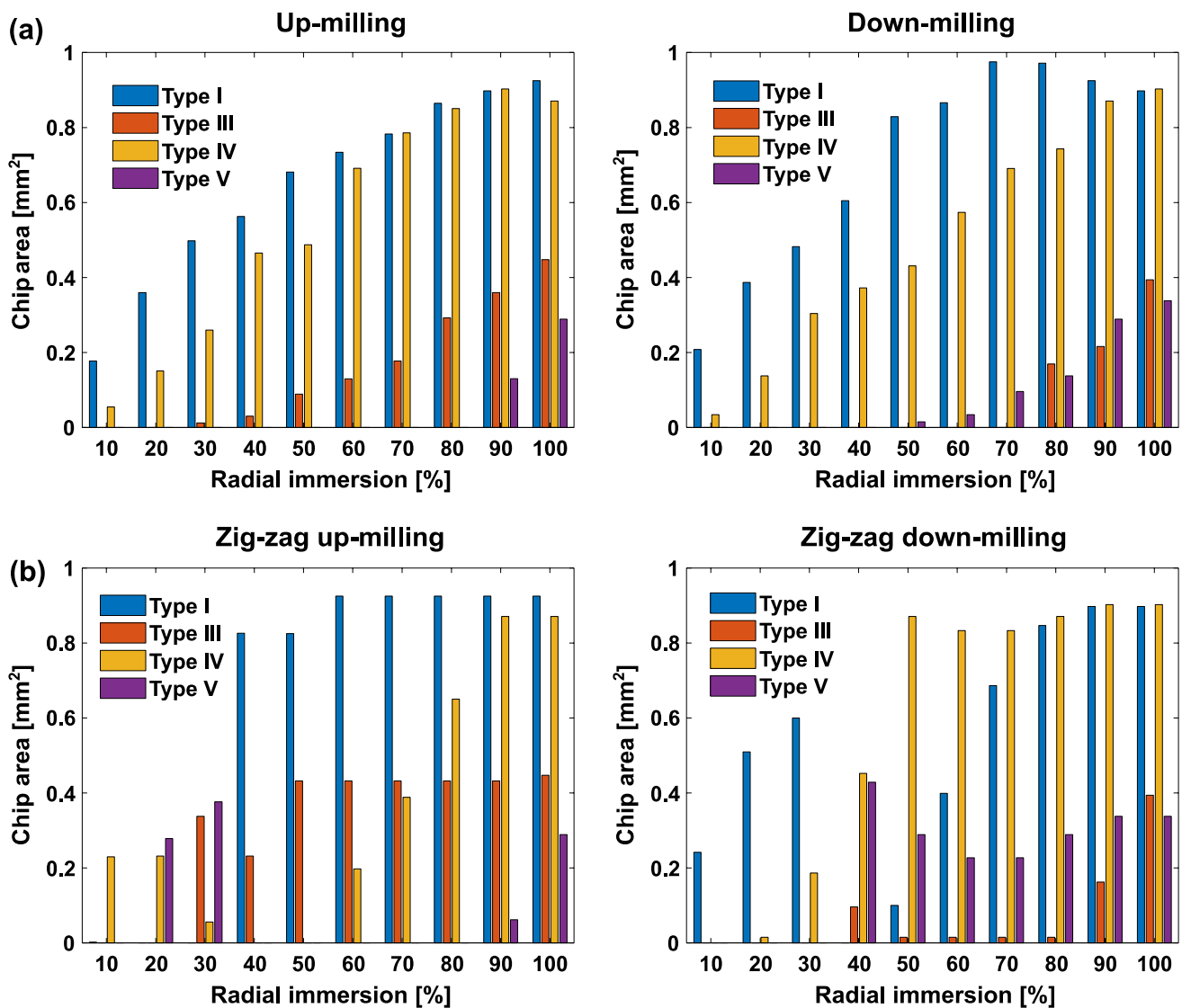
Fig. 16 Chip formation type as a function of radial immersion during milling in the optimal feed direction. **a** Up- and down-milling and **b** zig-zag milling

is lowest near the fiber cutting angle of 40°, and the surrounding chip formation is Type I; therefore, its portion is largest. In contrast, during chip formation in zig-zag milling, Type I is not dominant from 10 to 30% radial immersion in up-milling, whereas Type I is not dominant from 40 to 100% radial immersion in down-milling [Fig. 16b]. In zig-zag milling, up- and down-milling are considered simultaneously; thus, the dominant chip formation type is unclear when considered at only one of the two conditions. However, if the values of up- and down-milling of zig-zag milling are considered together, Type I is dominant.

Chip formation can significantly affect the machined surface. However, because chip formation has the greatest influence at the point where the machined surface is created, further research is needed to determine whether the

distributions in Fig. 16 are directly related to the machined surface quality. Therefore, the optimal feed direction is useful when cutting force and productivity are more important than quality (e.g., during roughing); in the context of finishing (where quality is essential), there is a need to consider chip formation near the machined surface. Further research is necessary because the shape and machining position of a CFRP workpiece are more difficult to adjust.

4 Conclusion

In this study, cutting force and chip formation were analyzed as functions of radial immersion, feed rate, and feed direction in zig-zag milling of CFRP using the cutting force

model. The specific cutting force decreased with increasing feed rate and chip thickness. This result resembles the size effect observed in metal machining; the behavior can be modeled by regression. In zig-zag milling, the optimal feed direction did not follow a continuous path; instead, it rapidly changed after 30% radial immersion. Furthermore, the cutting force reduction ratio changed to a parabolic form after 30% radial immersion. In zig-zag milling, the cutting force reduction ratio was large at approximately 75% radial immersion. Regarding chip formation type in the optimal feed direction, Type I chips were predominantly removed during both up- and down-milling. Individual analysis of the up- and down-milling components of zig-zag milling could not clearly identify the chip formation type, but Type I chip formation was dominant if up- and down-milling were considered in combination. This behavior occurred because Type I has the lowest specific cutting force.

The main results of the study are as follows.

1. The reduction ratio of cutting force in zig-zag milling is large at 75% radial immersion. Because this is a roughing condition, it is appropriate for optimization of the cutting force. The cutting force optimization method is commonly used in roughing conditions; with respect to CFRP, zig-zag milling is effective in a process focused on cutting force reduction and enhanced productivity.

2. With respect to unidirectional CFRP, the magnitude of the specific cutting force can substantially vary according to the CFRP specification; however, the effect of fiber cutting angle on specific cutting force is similar. Therefore, our cutting force prediction model-based analysis and optimization method can be applied to CFRP of various specifications. Some experiments are required to derive the specific cutting force, but once this is known it is possible to check the cutting force under various conditions via simulation. If it is difficult to obtain the specific cutting forces by experimentation, trends could be validated using data from this study.

3. More variables affect cutting force and chip formation in CFRP than in metals; the presence of these additional variables hinders experimental analysis. Additionally, cutting force prediction model-based analysis is more efficient because results measured under specific experimental conditions are only applicable to a limited range of conditions. This study used cutting force models to expand the scope of previous studies, which were limited to the development of cutting force models. The technology described here can be used in the development of CFRP cutting force optimization software.

4. In milling, according to the CFRP shape and machining part, up-, down-, and zig-zag milling may require individual or simultaneous consideration. Importantly, there are tool paths other than zig-zag milling; these paths can also be modeled based on up- and down-milling cutting force models. Therefore, the cutting force and chip formation analysis method presented in this study can be used to assess the cutting characteristics of more diverse CFRP milling approaches.

Author Contributions All authors read and approved the final manuscript.

Declarations

Competing interests The authors declare that they have no competing interests.

References

1. Seo, J. W., Kim, D. Y., Kim, D. C., & Park, H. W. (2021). Recent developments and challenges on machining of carbon fiber reinforced polymer composite laminates. *International Journal of Precision Engineering and Manufacturing, 22*, 2027–2044. https://doi.org/10.1007/s12541-021-00596-w

2. Poór, D. I., Geier, N., Pereszlai, C., & Xu, J. (2021). A critical review of the drilling of CFRP composites: Burr formation, characterisation and challenges. *Composites Part B: Engineering, 223*, 109155. https://doi.org/10.1016/j.compositesb.2021.109155

3. Choi, J. Y., Jeon, J. H., Lyu, J. H., et al. (2022). Current applications and development of composite manufacturing processes for future mobility. *International Journal of Precision Engineering and Manufacturing-Green Technology.* https://doi.org/10.1007/s40684-022-00483-3

4. Haddad, M., Zitoune, R., Eyma, F., & Castanie, B. (2014). Study of the surface defects and dust generated during trimming of CFRP: Influence of tool geometry, machining parameters and cutting speed range. *Composites. Part A, Applied Science and Manufacturing, 66*, 142–154. https://doi.org/10.1016/j.compositesa.2014.07.005

5. Hocheng, H., Puw, H. Y., & Huang, Y. (1993). Preliminary study on milling of unidirectional carbon fibre-reinforced plastics. *Composites Manufacturing, 4*, 103–108. https://doi.org/10.1016/0956-7143(93)90077-L

6. Hocheng, H., & Tsao, C. C. (2003). Comprehensive analysis of delamination in drilling of composite materials with various drill bits. *Journal of Materials Processing Technology, 140*, 335–339. https://doi.org/10.1016/S0924-0136(03)00749-0

7. Hintze, W., & Hartmann, D. (2013). Modeling of delamination during milling of unidirectional CFRP. *Procedia CIRP, 8*, 444–449. https://doi.org/10.1016/j.procir.2013.06.131

8. Abrão, A. M., Rubio, J. C. C., Faria, P. E., & Davim, J. P. (2008). The effect of cutting tool geometry on thrust force and delamination when drilling glass fibre reinforced plastic composite. *Materials and Design, 29*, 508–513. https://doi.org/10.1016/j.matdes.2007.01.016

9. Gaitonde, V. N., Karnik, S. R., Rubio, J. C., et al. (2008). Analysis of parametric influence on delamination in high-speed drilling of carbon fiber reinforced plastic composites. *Journal of*

Materials Processing Technology, 203, 431–438. https://doi.org/10.1016/j.matprotec.2007.10.050

10. Gaugel, S., Sripathy, P., Haeger, A., et al. (2016). A comparative study on tool wear and laminate damage in drilling of carbon-fiber reinforced polymers (CFRP). *Composite Structures, 155*, 173–183. https://doi.org/10.1016/j.compstruct.2016.08.004

11. Geier, N. (2020). Influence of fibre orientation on cutting force in up and down milling of UD-CFRP composites. *International Journal of Advanced Manufacturing Technology, 111*, 881–893. https://doi.org/10.1007/s00170-020-06163-3

12. Sheikh-Ahmad, J., Twomey, J., Kalla, D., & Lodhia, P. (2007). Multiple regression and committee neural network force prediction models in milling FRP. *Machining Science and Technology, 11*, 391–412. https://doi.org/10.1080/10910340701554873

13. Mullin, R., Farhadmanesh, M., Ahmadian, A., & Ahmadi, K. (2020). Modeling and identification of cutting forces in milling of carbon fibre reinforced polymers. *Journal of Materials Processing Technology, 280*, 116595. https://doi.org/10.1016/j.jmatprotec.2020.116595

14. Ning, H., Zheng, H., Zhang, S., & Yuan, X. (2021). Milling force prediction model development for CFRP multidirectional laminates and segmented specific cutting energy analysis. *International Journal of Advanced Manufacturing Technology, 113*, 2437–2445. https://doi.org/10.1007/s00170-021-06690-7

15. Wang, C., Zhang, X., Zhai, Z., & Chen, X. (2022). Parametric prediction model and periodic fluctuation interpretation of unidirectional CFRP edge milling force. *Composite Structures, 287*, 115387. https://doi.org/10.1016/j.compstruct.2022.115387

16. Kim, D. G., Jung, Y. C., Kweon, S. H., & Yang, S. H. (2022). Determination of the optimal milling feed direction for unidirectional CFRPs using a predictive cutting-force model. *International Journal of Advanced Manufacturing Technology, 123*, 3571–3585. https://doi.org/10.1007/s00170-022-10309-w

17. Wang, H., Ning, F., Hu, Y., et al. (2018). EDGE trimming of CFRP composites using rotary ultrasonic machining: Effects of ultrasonic vibration. In *ASME 2018 13th Int Manuf Sci Eng Conf MSEC 2018* (Vol. 4, pp. 1641–1653). https://doi.org/10.1115/MSEC2018-6362

18. Slimane, A., Slimane, S., Kebdani, S., et al. (2019). Parameters effects analysis of rotary ultrasonic machining on carbon fiber reinforced plastic (CFRP) composite using an interactive RSM method. *International Journal on Interactive Design and Manufacturing, 13*, 521–529. https://doi.org/10.1007/s12008-018-0518-0

19. Kannan, S., & Pervaiz, S. (2020). Surface morphology of inclined CFRP holes when machined under cryogenic environment. *Materials and Manufacturing Processes, 35*, 1228–1239. https://doi.org/10.1080/10426914.2020.1762208

20. Kumar, D., & Gururaja, S. (2020). Machining damage and surface integrity evaluation during milling of UD-CFRP laminates: Dry vs. cryogenic. *Composite Structures, 247*, 112504. https://doi.org/10.1016/j.compstruct.2020.112504

21. Kumar, D., Gururaja, S., & Jawahir, I. S. (2020). Machinability and surface integrity of adhesively bonded Ti/CFRP/Ti hybrid composite laminates under dry and cryogenic conditions. *Journal of Manufacturing Processes, 58*, 1075–1087. https://doi.org/10.1016/j.jmapro.2020.08.064

22. Kim, G., Kim, T. G., Lee, S. W., & Min, B. K. (2022). Effect of workpiece preheating on tool wear and delamination at the hole exit in high feed drilling of carbon fiber reinforced plastics with diamond-coated tools. *Journal of Manufacturing Processes, 74*, 233–243. https://doi.org/10.1016/j.jmapro.2021.12.013

23. Toh, C. K. (2005). Comparison of chip surface temperature between up and down milling orientations in high speed rough milling of hardened steel. *Journal of Materials Processing Technology, 167*, 110–118. https://doi.org/10.1016/j.jmatprotec.2004.10.004

24. Bouzakis, K. D., Makrimallakis, S., Skordaris, G., et al. (2013). Coated tools' performance in up and down milling stainless steel, explained by film mechanical and fatigue properties. *Wear, 303*, 546–559. https://doi.org/10.1016/j.wear.2013.04.014

25. Laamouri, A., Ghanem, F., Braham, C., & Sidhom, H. (2019). Influences of up- and down-milling on surface integrity and fatigue strength of X160CrMoV12 steel. *International Journal of Advanced Manufacturing Technology, 105*, 1209–1228. https://doi.org/10.1007/s00170-019-04280-2

26. Huo, G., Jiang, X., Su, C., et al. (2019). CNC tool path generation for freeform surface machining based on preferred feed direction field. *International Journal of Precision Engineering and Manufacturing, 20*, 777–790. https://doi.org/10.1007/s12541-019-00084-2

27. Shi, K., Liu, N., Wang, S., & Ren, J. (2019). Effect of tool path on cutting force in end milling. *International Journal of Advanced Manufacturing Technology, 104*, 4289–4300. https://doi.org/10.1007/s00170-019-04120-3

28. Mali, R. A., Gupta, T. V. K., & Ramkumar, J. (2021). A comprehensive review of free-form surface milling—Advances over a decade. *Journal of Manufacturing Processes, 62*, 132–167. https://doi.org/10.1016/j.jmapro.2020.12.014

29. Wang, J., Jiang, R., Wu, Z., et al. (2023). Investigation of surface integrity up-milling magnesium oxide particle reinforced wood-based composite. *International Journal of Precision Engineering and Manufacturing*. https://doi.org/10.1007/s12541-022-00737-9

30. Kang, G., Kim, J., Choi, Y., & Lee, D. Y. (2022). In-process identification of the cutting force coefficients in milling based on a virtual machining model. *International Journal of Precision Engineering and Manufacturing, 23*, 839–851. https://doi.org/10.1007/s12541-022-00677-4

31. Fu, X., Song, K., Kim, D. M., et al. (2022). Geometrical simulation model for milling of carbon fiber reinforced polymers (CFRP). *International Journal of Precision Engineering and Manufacturing, 23*, 1237–1260. https://doi.org/10.1007/s12541-022-00681-8

32. Pereszlai, C., Geier, N., Poór, D. I., et al. (2021). Drilling fibre reinforced polymer composites (CFRP and GFRP): An analysis of the cutting force of the tilted helical milling process. *Composite Structures, 262*, 113646. https://doi.org/10.1016/j.compstruct.2021.113646

33. Altintas, Y. (2004). Manufacturing automation: Metal cutting mechanics, machine tool vibrations, and CNC design.

34. Sheikh-Ahmad, J. Y. (2009). *The machining of polymers composites*. Springer.

Dong-Gyu Kim is a Mechanical Engineering Ph.D candidate at Kyungpook National University and a senior researcher at Daegu Mechatronics & Materials Institute (DMI) in Daegu, Korea. His research interest is intelligent manufacturing systems and machining process.

Seung-Han Yang Seung-Han Yang received the Ph.D. degree in mechanical engineering from the University of Michigan, Ann Arbor, Michigan, USA. He is currently a professor in the School of Mechanical Engineering, Kyungpook National University. His research interest is intelligent manufacturing systems and CAD/CAM.